Local elastic properties of carbon nanotubes in the presence of Stone-Wales defects

N. Chandra, S Namilae and C.Shet

Department of Mechanical Engineering

FAMU-FSU College of Engineering

Florida State University

Tallahassee, Fl 32312

(April 11, 2003)

Abstract

Carbon nanotubes (CNT) are being contemplated as reinforcements for next generation of composite materials. Stress and strain measures at atomic scale are required to study the effect of inhomogeneities in nanotube based structures. In this work, we have adapted three different stress measures at atomic scales and introduced a strain measure as energetically conjugate quantities. These measures are validated for defect free nanotubes and are then used to study the mechanics of 5-7-7-5 topological defects in various single wall nanotubes. It is observed that there is a decrease in load carrying capacity in the defected region, and the decrase can be attributed to the kinetics and the changes in kinematics in the vicinity of the defects.

I. INTRODUCTION

The exceptional mechanical properties of carbon nanotubes (CNTs) and their potential use in structural components and devices have stimulated great interest and extensive research, ever since their discovery by Iijima[1] in 1991. The stiffness and strength of CNTs are in the range of TPa and GPa respectively, while the nearest competing material exhibit these properties in the range of GPa and MPa respectively. Also the fact that CNTs are extremely light weight compared to other materials make them potential candidates as reinforcing fibers in super strong composites. Before they can be applied in real nanocomposites, strength and stiffness of CNTs as stand alone units and their ability to transfer loads between matrix and the nanotubular fibers through nanoscale interfaces needs to be clearly understood. At the heart of the problem is the very definition of strength and stiffness at these scales. Strength and stiffness are defined based on stresses and strains at the macroscopic continuum level and these definitions are ambiguous at the nanoscopic level. This issue is neither philosophical nor pedagogical but one of practical relevance as will be illustrated in this paper. Widely reported computational and experimental results of CNT strength

and stiffness are based on averaged quantities computed or measured at the length scale of nanotube which is many orders greater than the local atomic dimensions. Though these averaged quantities may lead to acceptable properties for a few idealized configurations, local measures are required to unequivocally determine certain extremum behavior such as inelasticity, damage, fracture and failure. Such is the case when we need to study the origin and effect of deviation from the regular hexagonal arrangement of carbon in graphene sheet or in carbon nanotubes. Local mechanical behavior, for example in a 5-7-7-5 Stone-Wales defect is entirely different from that of a region away from the defect, all within the same nanotube subjected to a far field force. The relation between the average and local behavior is a well-known problem in the macro world but is manifested with even more vigor in the CNTs based nano-world, and is the subject of the present paper. Though we have focused on single walled CNT in this work, the methodology developed here is equally applicable to multi-walled CNTs. Since we mainly deal with single wall carbon nanotubes in this work, the term CNT refers to single wall carbon nanotube unless indicated otherwise.

Experimental observations have revealed that topological defects such as 5-7-7-5 Stone-Wales defect are commonly present in nanotubes.[2] These local defects can alter not only the inelastic properties but also the elastic properties, e.g., Young's modulus and Poisson's ratio. Consequently, these defects may alter the longitudinal, lateral stiffnesses, and flexural rigidity in response to tension, torsion and bending respectively. It should be noted that analogous point or line defects (vacancies, substitutional atoms and dislocations) in a bulk crystalline materials tend to influence only the inelastic properties because these type of defects though quite large in number are still extremely small volumetrically. Because of the unique planar hexagonal mesh-like structure of the carbon nanotubes, topological defects can alter the deformation response and hence the elastic properties. In addition, these can also be the potential sites where irreversible mechanical response initiates.[3] While these assertions are true even for planar graphene sheets, when rolled as carbon nanotubes these defects locally alter the curvature of the tubes causing further nonlinear effects. Consequently, they respond differently not only when the diameter varies, albeit to a lesser extent, compared

to the chirality where the rolling orientation directly affects the geometry near the defects.

Studies have shown that defects in CNTs may not only affect the mechanical properties, but electronic, magnetic and hybridization characteristics and hence needed to be understood thoroughly.[4–6] Also the transition in the Y-junction contemplated in CNT based molecular electronics is achieved through the incorporation of many 5-7-7-5 defects either by design or otherwise[7] . Similarly, transition of nanotubes from one diameter to another can be achieved by locating a few of these defects strategically in the transition region. In addition, when nanotubes are used as fibers in nanocomposites interfacial bonding may preferably occur in these defected regions based on energy considerations. Thus when studying load transfer issues in CNTs, understanding the mechanics of these zones is critical. Another area of potential application of CNTs is in the effective storage of hydrogen for possible use in fuel cells. Here again the propensity of hydrogen penetrating a defected region and entering the tube is higher than regular regions.

In this paper, we introduce the definitions of atomic stress and atomic strain quantities as applicable to carbon nanotubes. Though these stress measures have already been used to compute stresses in a general three-dimensional crystalline materials, their application to carbon nanotubes is new and entails certain re-evaluation of what constitutes the proper volume in a planar configuration. We have formulated a methodology to evaluate the kinematic measure of atomic strain specifically for carbon nanotubes. Strain at the atomic level is still defined as the spatial gradient of the displacement field; the displacement field is expressed in terms of atomic displacements and interpolation functions. These measures are applied to CNTs with and without 5-7-7-5 Stone-Wales defects. Local stress -strain response in the defected and the perfect regions are then examined. It is observed that the defect produces stress and strain concentration effects in the vicinity of the defect due to changes in the geometric configuration and concomitant force fields. The *local stiffness* substantially decreases in the defected region and the mechanics of why this happens is examined in terms of both the kinematics and kinetics.

II. ATOMIC LEVEL STRESS MEASURES

Stress is a measure defined to quantify the internal resistance of material to counter external disturbances. These external disturbances can be either mechanical, thermal, electrical, magnetic or gravitational in nature. While mechanical loads appear as forces and moments at the surfaces of the body, other loads are distributed throughout the volume as body forces. Stress in a simplified sense can be construed as force over an infinitesimal area as the area tends to zero in the limiting process. It is implied in this definition that force acting over the infinitesimal area is uniform leading to a unique state of stress. Without loss of generality this concept of uniform force over an infinitesimal volume can be extended to the three dimensional state of stress with forces acting on the surfaces of the cube.

When we define stress at a point, in the sense of continuum mechanics we implicitly assume that a homogenous state of stress exists within the appropriately chosen infinitesimal volume surrounding that point. As we apply this concept to *discrete lattice mechanics,* we need to identify a volume around a given point over which the stress becomes homogeneous. Such a selection of appropriate volume clearly depends on the degree of stress heterogeneity existing at the material in question. It should be noted that the heterogeneity in the stress state can be caused either due to the heterogeneity in the material (e.g. defects such as inclusions) or due to inhomogeneous loading conditions (e.g. bending). If stress in a selected volume has a very sharp spatial gradient, than we are required to choose smaller and smaller volume to evaluate the stress quantity with a clear objective of choosing the largest possible volume to satisfy the condition of homogeneity within that volume.

In this context there have been various formulations of stress in molecular dynamics such as virial stress,[8] BDT or atomic stress,[9] Lutsko stress,[10,11] mechanical stress by Cheung and Yip.[12] We invoke these various definitions of stress measures with different volumes of interrogation and apply them to carbon nanotubes in a molecular dynamics formulation based on Brenner potential.[13] The most commonly used stress measure at atomic scale is virial stress[8] (Σ_{ij}). For a pair potential V this can be expressed as

$$\Sigma_{ij} = \frac{1}{\Omega^{Tot}} \sum_{\alpha=1,n} \left(\frac{1}{2} m^{\alpha} v_i^{\alpha} v_j^{\alpha} + \sum_{\beta=1,n} \frac{r_{\alpha\beta}^i r_{\alpha\beta}^j}{|r_{\alpha\beta}|} \frac{dV}{dr_{\alpha\beta}} \right). \quad (1)$$

Here i, j denote the indices in Cartesian coordinate system 1, 2 and 3, while α and β are the atomic indices. The summation is over all the atoms occupying total volume Ω^{Tot}. m^{α} and v^{α} denote the mass and velocity of atom α. $r_{\alpha\beta}$ is the distance between atoms α and β. The term $\frac{dV}{dr_{\alpha\beta}}$ is the scalar of force exerted on atom α by atom β. Without loss of generality this expression can be rewritten for potentials dependent on bond angles such as bond order potentials as:

$$\Sigma_{ij} = \frac{1}{\Omega^{Tot}} \sum_{\alpha=1,n} \left(\frac{1}{2} m^{\alpha} v_i^{\alpha} v_j^{\alpha} + \sum_{\beta=1,n} r_{\alpha\beta}^j f_{\alpha\beta}^i \right). \quad (2)$$

where $f_{\alpha\beta}^i$ is the force on atom α due to atom β resolved in ith direction. We have used this form to calculate virial stress. A similar form for atomic stress has been used for Si modeled with Tersoff potential by Yu and Madhukar.[14] Based on the preceding discussion regarding volume it may be noted that this stress formulation is strictly valid only when homogenous stress state exists in the entire volume of the simulation box. For example, this measure would be valid for uniformly loaded nanotubes without defects.

Above definition of bulk stress has been extended to one atomic volume by Basinski, Deusberry and Taylor[9] to define atomic stress (also called BDT stress). This is based on the assumption bulk stress measure would be valid for a small volume Ω^{α} around an atom α. This definition of atomic stress $\left(\sigma_{ij}^{\alpha}\right)$ for atom α can be expressed as:

$$\sigma_{ij}^{\alpha} = \frac{1}{\Omega^{\alpha}} \left(\frac{1}{2} m^{\alpha} v_i^{\alpha} v_j^{\alpha} + \sum_{\beta=1,n} r_{\alpha\beta}^j f_{\alpha\beta}^i \right). \quad (3)$$

Theoretically, the above definitions are valid only for homogenous systems, though BDT stress gives a fair indication of the nature of stresses in systems with defects and has been used to study point defects and grain boundaries in a number of metallic systems.[9,15,16] Total volume and volume of single atom are required for the calculation of virial and BDT stresses. Further to ensure consistency

$$\Sigma_{ij} = \frac{1}{\Omega^{Tot}} \sum_{\alpha} \sigma_{ij}^{\alpha} \Omega^{\alpha}. \quad (4)$$

The total volume has been used extensively in the computation of elastic modulus based on energy approach (See references in Table. I). We have used the most commonly used volume $\Omega^{tot} = \pi dtl$ where d is the diameter, l is the length and $t = 3.4\ \overset{o}{A}$ is the interplanar spacing in graphite. Atomic volume has been computed based on interatomic distance ($1.42\ \overset{o}{A}$ in undeformed tubes) and interplanar spacing ($3.4\ \overset{o}{A}$).

Other definitions of stress have been advanced by Lutsko[10] and Cheung and Yip[12] to study inhomogeneous systems. According to Cheung and Yip's definition, mechanical stress is calculated as sum of time rate of change of momentum flux and forces divided by area across particular surface of interest. The concept of local stress advanced by Lutsko and extended by Cormier et al.[11] is based on the local stress tensor of statistical mechanics. Further this definition has been shown to conserve linear momentum. Lutsko stress $\left(\sigma_{ij}^{L}\right)$ can be expressed as:

$$\sigma_{ij}^{L} = \frac{1}{\Omega^{Avg}} \sum_{\alpha=1,n} \left(\frac{1}{2} m^{\alpha} v_i^{\alpha} v_j^{\alpha} + \sum_{\beta=1,n} r_{\alpha\beta}^{j} f_{\alpha\beta}^{i} l_{\alpha\beta} \right). \tag{5}$$

Here $l_{\alpha\beta}$ denotes the fraction of the length of α-β bond lying inside the averaging volume Ω^{Avg}. Further, this averaging volume can be a small part of the total volume possibly containing defects. Lutsko stress has been used to evaluate local elastic properties of grain boundaries in metals. Cormier and coworkers[11] have recently shown that this measure gives a better match for continuum solution of inclusion problem.

In bulk materials the averaging volume (for Lutsko stress) is typically considered as a spherical volume, though the derivation of the stress tensor places no such restriction. We have considered averaging volume as shown in Fig. 1 for this calculation.

In summary, Virial stress can be used if the stress state is homogenous in the entire volume (of simulation cell); Lutsko stress can be computed for a partial volume and the homogeneity restriction is still applicable to that volume. If stress needs to be computed around a single atom, then BDT stress can be used. Here again homogeneity is assumed in the volume in which stress is computed. In the converse, if inhomogeneity exists then the choice of the stress measure depends on the extent of spatial inhomogeneity. For example if

we need to examine the overall effect of a 5-7-7-5 Stone-Wales defect, we need to use Lutsko stress. If we are further interested in the role of specific atom in the defected region, then we need to use BDT stress to capture the physics of the problem.

In spite of the fact that these various definitions have been used with regularity in studying metallic systems (both for EAM and pair potentials), and some non metallic systems such as Si, Ge[14], to the best of our knowledge they have not been used for carbon nanotubes. For carbon nanotubes, Halicioglu[17]has obtained the atomic stress values in carbon nanotubes based on the strain energy consideration using

$$\sigma_{ij} = \frac{1}{\Omega}\frac{\partial E^{\alpha}}{\partial \varepsilon_{ij}}. \tag{6}$$

Here E^{α} is the strain energy and ε_{ij} is the corresponding strain component. This measure is used for the entire tube and requires knowledge of conjugate strain. Belytschko and coworkers[18] calculate stress based on applied forces and cross sectional area of nanotube. Xia and coworkers[19] calculate stress based on pressure exerted by hydrogen atoms in the nanotube and averaged increase in the dimensions of the nanotube.

The prevailing methods of evaluating elastic moduli and stress-strain behavior of nanotubes implicitly assume that homogenous state of stress exists allowing them to use energy to compute the modulus. Further they need to know the value of strain and assume that strain is constant throughout the domain. This would not pose any problems for nanotubes without defects under uniaxial loading. We show in the later sections that when the condition of homogeneity is violated, as in a defected system, or in the case of multiaxial state of loading local stress and strain measures would prove to be more useful than global energy based approaches. Now we proceed to develop the kinematic or strain measure for nanotubes at atomic scale.

III. ATOMIC LEVEL STRAIN AND ENERGY MEASURES

In the description of continuous media, the thermomechanical behavior of materials is usually prescribed by relating the kinetic quantity at a given material point (or particle) to

a kinematic quantity through a constitutive equation. For example, in the Hooke's law for isotropic materials the kinematic quantity strain, ε, is related to the kinetic measure stress, σ, using the simple relation $\sigma = E\varepsilon$ where E is the Young's modulus. This modulus is usually evaluated in a uniaxial tensile test where the stress state is uniaxial ($\sigma_{11} = \sigma$) but the strain state is multiaxial ($\varepsilon_{11} = \varepsilon; \varepsilon_{22} = \varepsilon_{33} = -\nu\varepsilon$) and the modulus is $E = \frac{\sigma_{11}}{\varepsilon_{11}} = \frac{\sigma}{\varepsilon}$. The strain energy associated with the deformation is given by

$$dW = \sigma d\varepsilon \Rightarrow W = \frac{\sigma^2}{2E} = \frac{E\varepsilon^2}{2}. \tag{7}$$

If Young's modulus is a constant then the stress-strain response is linear and strain energy in equation (7) is valid. Such is the case for a linear elastic isotropic material. The above equation illustrates the fact that in order to evaluate Young's modulus in a linear elastic model, only any two of the variables, stress, strain and energy are independent. While we pursue to evaluate the former two, many workers have used energy and strain to obtain these quantities under homogenous conditions. Young's modulus can be evaluated using energy and some strain measure using the equation,

$$E = \frac{2W}{\varepsilon^2} \quad \text{or in general terms as,} \quad E = \frac{\partial^2 W}{\partial \varepsilon^2}. \tag{8}$$

In the above equation selection of any strain measure ε yields a corresponding modulus E, though it can be easily noticed that the pairs are not unique. For example, if one were to select a new measure ϵ^* and then evaluate E^* then this new modulus will be quite different as shown below.

$$\epsilon^* = \alpha\varepsilon \qquad \sigma^* = \beta\sigma \Rightarrow E^* = \gamma E \quad \text{where} \quad \gamma = \frac{\beta}{\alpha} \text{ given that } \alpha\beta = 1. \tag{9}$$

The above equation holds good for any arbitrary value of α and β. It is thus clear that one can get quite different values of Young's modulus based on the selection of strain measure or stress measure. For the more general case of anisotropic elastic materials, if W is assumed to be a function of only current deformed state and independent of the history of deformation then the material is hyperelastic with

$$C_{ijkl} = \frac{\partial^2 W}{\partial \varepsilon_{ij} \partial \varepsilon_{kl}}, \tag{10}$$

where C_{ijkl} are the components of fourth order elasticity tensor and ε_{ij} are the components of strain tensor. Unfortunately for the above equation to be consistent with the usual elasticity tensor components one needs to identify ε_{ij} as the components of the frame invariant Green-Lagrange strain tensor. Thus evaluating stiffness components using equation (10) or equation (8) has several shortcomings.

1. The magnitude of the Young's modulus even for isotropic cases, depends on the choice of strain measure, as shown in equation (9).

2. In using equation (7) the carbon nanotubes exhibit directional independence in their material orientations. Clearly this is not the case as the mechanical response of a zig-zag tube is different from that of an armchair tube. Thus the equation presumes that material is isotropic which is incorrect.

3. The equation implicitly assumes that a state of homogeneous deformation occurs throughout the volume of interrogation which is not always the case.

4. We need to implicitly assume that strain energy density function exists for these classes of materials.

5. We need to assume that the internal strain energy in the material is always equal to the change in potential energy as given by the interatomic potentials. This would not be true for simulations at finite temperature.

Based on the above argument, the proposed method of evaluating local stresses and strains is a better approach to the problem. Strain is a measure of the deformation suffered by a body and is typically measured by the relative changes in length and angles of line segments of the deformed configuration compared to the original. The simplest form of strain is the uniaxial strain defined by $\varepsilon = (L - L_o)/L_o$, where L is the current length and

L_o is the original length. Though this form of strain has been used for nanotubes,[18,20] it may not be sufficient to represent multiaxial strain state or prove adequate for inhomogeneous distributions.

A more general measure that is applicable to large deformation and finite rotation cases is the deformation gradient tensor F which relates deformed configuration x to undeformed configuration X given by

$$F = \frac{d\mathsf{x}}{d\mathsf{X}}. \tag{11}$$

Displacement u of a given atom can be expressed as

$$\mathsf{u} = \mathsf{x} - \mathsf{X}. \tag{12}$$

An infinitesimal strain measure ε defined as

$$\varepsilon = \frac{\partial \mathsf{u}}{\partial \mathsf{X}} = (\mathsf{F} - \mathsf{I}), \tag{13}$$

is used in this work. For a theoretically consistent formulation one needs to identify a set of frame invariant stress and strain measures that are not only conjugate quantities but are evaluated in the same configuration, either in the undeformed or the deformed state. There are many choices available and the selection criterion is beyond the scope of this paper. However, if we choose to use the deformed configuration as our reference state, then we can use Cauchy stress and Almansi strain as the conjugate quantities. Further, Almansi strain can be approximated to the small strain measure presented above (equation 13), if the strains are not large and if the rigid body rotations during the deformations are limited.

The computational methodology for calculating strains is as follows: Defect free nanotube can be considered as a mesh of hexagons. Each of these hexagons can be treated as containing four triangles. A local coordinate system $\left(X'Y'Z'^{\emptyset}\right)$ is constructed for each of these triangles with centroid as origin and local Z' axis is along the length of tube (See Fig. 2), the local Y′ is coincides with the radial direction of the centroid of the triangle. Local X' is obtained as cross product of Z' and X' axes, so that atoms lie on $X'^{\emptyset} - Z'^{\emptyset}$ plane. The

in-plane strains ($\varepsilon_{z^\theta}, \varepsilon_{x^\theta}, \varepsilon_{z^\theta x^\theta}$) for this configuration can be evaluated using displacements of atoms i, j and l ($u_i, v_i, ..$) which form the triangle as

$$\left\{ \begin{array}{c} \varepsilon_{z^\theta} \\ \varepsilon_{y^\theta} \\ \gamma_{z^\theta y^\theta} \end{array} \right\} = [B] \left\{ \begin{array}{cccccc} u_i & v_i & u_j & v_j & u_l & v_l \end{array} \right\}^T$$

where $[B]$ is the matrix of the gradient of the interpolation functions[21]. Once the strains of the triangular facets are obtained strains in hexagons are evaluated as area weighted average of triangles contained in the hexagons. In the case of tubes with 5-7-7-5 defect the mesh described above contains heptagons and pentagons along with hexagons. These pentagons and heptagons are composed of three and five triangular facets respectively. Strain at each atomic location is evaluated as average of three hexagons (or heptagons/pentagons) that encompass the concerned atom.

IV. RESULTS AND DISCUSSION

In this section we present results obtained from molecular static simulations using conjugate gradient algorithm and Brenner potentials. Periodic boundary conditions were applied to model tubes of infinite length. For simulating CNTs under uniaxial loading, displacements were applied to the atoms in the longitudinal direction. Stress, strain and energy measures at the local and global levels were computed for all cases. In order to validate the new local stress and strain measures, a perfect (9,0) CNT was analyzed. Once validated, these measures are used to study the 5-7-7-5 defect in tubes with different diameters and chiralities.

In zig-zag (n,0) nanotubes 5-7-7-5 defects can be manifested in two different types, type I and type II, as shown in the Fig. 3 and 4. In type I defect, a horizontal bond of a hexagonal network is rotated by 90^o so that when the defect is formed, two of the hexagons are transformed to two heptagons and two pentagons, placed symmetrically about x (or

$y) - z$ axes. In the type II defect heptagons and pentagons are asymmetric with x (or $y) - z$ axes.

A. Validation of stress and strain measures

When subjected to a far field load on a defect free homogenous state of stress and strain exist. Strain calculations based on triangular facet approach give consistent results for tubes with different chiralities and diameters. Also the three stress measures yield consistent stress values. For a tube with uniform strain, the variation in BDT stress (computed for each atom) from atom to atom is negligible, and the magnitude of BDT stress and virial stress are found to be identical. For homogenous systems by, definition virial and BDT stresses coincide, since the volume Ω^{tot} in equation (2) is equal to $n\Omega^{\alpha}$ in equation (3) where n is the number of atomsin the system. When Lutsko stress is computed, a volume slightly larger than twice cutoff radius is used. The additional $l^{\alpha\beta}$ term (see equation (4)) leads to a small difference between lutsko and virial stresses. If we choose larger volume for lutsko stress, the difference reduces and completely vanishes when the interrogating volume is equal to total volume. However, the slope of stress-strain curve in all the three cases is identical.

It is interesting to note that the strain values in the triangles are not necessarily equal to applied strain values. Though the magnitude of strain in adjacent triangles is different, the weighted average of strain in any hexagon is same and is identical to the applied strain. consequently, every atom experiences same state of strain. The variation of strain state within the hexagon (in different triangular facets) is a consequence of different orientations of interatomic bonds with respect to applied load axis.

Further, to validate the applicability of the three stress measures and the strain measure, stress-strain curves are plotted for a perfect (9,0) CNT under uniaxial tension. Fig. 5 shows the stress-strain curves based on virial, Lutsko and BDT stress, measured in longitudinal (Z) direction and longitudinal strain ε_z. The Young's modulus is evaluated as the slope of stress-strain curve at zero strain (initial tangent). We obtain a Young's modulus value of

1.002 TPa for (9,0) CNT. This compares favorably with values published in the literature as shown in Table. I. Though there is a wide variation in the value of the Young's modulus (0.5 to 5.5 TPa), based on different computational and experimental approaches, the value centers around 1TPa which compares well with this investigation.

Having validated the stress and strain measures, in the next section (B) we present the mechanical response of nanotubes with 5-7-7-5 defects. The results are then followed by a discussion of interesting observations in section (C).

B. Deformation of nanotubes with 5-7-7-5 defect

Fig. 6 shows the variation of Lutsko stress σ_{33} along the length of the (9,0) tube. The tube has a symmetric 5-7-7-5 defect placed in the middle of the tube. Nanotube is divided into seven segments along the length, and a strip of atoms in each segment as shown in Fig. 1, is selected for computing average stresses and strains. It can be clearly observed from the Fig. 6 that there is a stress amplification in the central segment which contains the defect. We note that even at zero strain level, a stress value of about 15 GPa is observed at the defect, analogous to residual stresses at macro scales. As the strain level increases, the stress concentration factor (defined as the ratio of peak stress to average stress) decreases.

Fig. 7 shows the variation of longitudinal strain ε_{33} along of length of CNT for different strain levels. At 0% external strain, the local strain at all the points are equated to zero and forms the reference configuration against which further deformation is measured. Though it is possible to use other reference states (for example, a defect-free CNT with a hexagonal network) the present choice is preferred since displacements are identically zero. With this definition of the initial state, strain is zero, in not only defect free hexagons, but also in pentagons and heptagons.

From Fig. 7, it can be observed that magnitude of strain increases at the defect and is uniform away from the defect. The longitudinal strain response is considerably different from that of the stress. The strain concentration (defined as the ratio of local to the global

average) increases with increase in externally applied load, while the stress concentration is found to decrease with increasing applied strain. The shear strains are equal to zero in nanotubes without defects but a small amount of shear (about one tenth of applied strain) is present in defected tubes. This effect is found to extend to the areas adjoining defected region.

Since the local values of stress and strain vary for each of the atoms in the defected region, it is useful to examine the spatial variation of these quantities using a contour plot. Fig. 8 shows the stress and strain contour plots near the defected region for various applied strains. Stress contours are based on BDT (atomic) stresses and correspond to the strain states which are also computed at each atom. Both stress and strain contours show concentration effects on the rotated bond that engenders the type I defect. Though not shown here, peak stress occurs at the defect even at zero applied strain and this corresponds to the stress caused due to the presence of defect. Contour plots show that both stress and strain values monotonically increase though there are some differences in their responses.

Use of Lutsko stress enables us to examine the stress-strain response of the defected region per se and compare it with the properties of defect free CNT. Fig. 9 shows lutsko stress-strain curves for defect free (9,0) nanotube (plot a) and compares it with the Lutsko stress-strain curves of the defected regions. From this plot it can be observed that there is a drop in stiffness at the defect. The stiffness of region with type I defect (plot b) is 0.621 TPa and that of type II defect (plot c) is 0.627 TPa in contrast to a much higher Young's modulus value of 1.002 TPa for defect free CNT.

We now proceed to compare the effect of defects on mechanical properties for various diameters. The numerical values of stiffness of defected regions in different CNTs are tabulated in Table. II and Fig. 10 shows the stress-strain curves. There is only a marginal difference in the local stiffness values for various (n,0) CNTs.

C. Discussion

It is quite noteworthy that even for fully equilibrated defect free CNTs, a non zero stress of few GPa is observed at zero strain (see Figs. 9 and 10). This can be construed as residual stresses which are defined as self equilibrating internal stresses even in the absence of external loads (thermal or mechanical).If these non-zero residual stresses are caused by the geometry of formation, then the magnitude of stress should depend on the diameter. Fig. 11 shows the variation of zero-strain stresses with inverse of radius for various (n,0) type CNTs. It can be seen from Fig. 11 that these stresses decrease monotonically with radius of CNTs and approach zero for infinite radius i.e. graphene sheet. Since these stresses vanish for graphene sheet and increase with curvature, these stresses can be considered as the formation stresses relative to graphene sheet and hence formation induced residual stresses. The residual stresses should also correspond to strain energy relative to graphene sheets and are supported by the results of Robertson and coworkers[34].

Further, in the nanotubes with defects at zero strain, there is an additional stress (and hence energy) that corresponds to the formation of defects (See Fig. 6). Thus in defected regions residual stresses arise both due to the curvature and defect formation. Atomic structure in the vicinity of defect has more deviation from perfect SP2 hybridized structure (Planar with bond-angles of 120^o as in graphene sheet) compared to perfect regions of CNT. While stresses due to curvature are influenced by the radius of CNT, stresses due to defect formation are affected by the type of defect.

It is observed in Fig. 6, that stress concentration due to the presence of defects decreases at higher strains. In other words with increased strain levels, the effect of defect in enhancing the local stress level decreases. Several investigators[35–39] have observed spontaneous formation of defects at higher strains. These studies have shown that the defected structures have lower energy at higher strains[38]. Lowered energy is manifested as lowered stress concentration effect.

Contrary to stress concentration, strain concentration at the defect increases as applied

strain is increased (see Fig. 7). In order to understand this, let us look more closely at the deformation pattern away from the defect and near the defect. Consider a defect free region as shown in Fig. 12(b). The basic hexagonal network is expected to stretch under the action of axial load. As a result there is a reduction in bond angles such as $\widehat{UPQ}$ and a corresponding increase in bond angles such as $\widehat{PQR}$. Geometrical constraint due to hexagonal nature of mesh entails that increase in angles $\widehat{PQR}$ be about two times the decrease in angles $\widehat{UPQ}$ as observed in Fig. 13. In addition, the bonds in the line of action of axial load such as PY are expected to stretch and bonds such as PQ stretch and rotate. The deformation induces predominantly longitudinal strains and compressive lateral strains due to the Poisson's effect. Shear strains are caused by angle changes between any two perpendicular lines before and after deformation. Since the hexagon is extended in one direction and compressed in the other, this type of deformation does not induce any shear strain.

Now consider the region with 5-7-7-5 defect as shown in Fig. 12(a). The defected regions comprise irregular heptagons and pentagons. Also the angles between bonds have considerable deviation from perfect sp2 structure (with bond angle 120^o). It is intuitive to expect that deformation of this high energy structure would occur by rearranging of bond angles rather than bond lengths. Fig. 14 shows the bond angle changes for selected atoms near the defected region with respect to applied strains. Significant variation in bond angles is observed; for example there is an angular variation of up to 11% in $\widehat{ABH}$ at applied strain of 8% in contrast to maximum angle variation of 4% in defect free structure for (9,0) CNT. Larger changes in bond angles induce a larger component of rotation to the strain leading to higher longitudinal strains in the defected region. In addition, irregularity of the heptagons and pentagons combined with large angular changes results in higher shear strain. As a result of these larger strains at lower stresses, the local stiffness of defected region is much lower than corresponding defect free regions. A fluctuation in radius of curvature is observed at the defect. For example the radius of curvature at the defect varies from 3.45 to 3.53 $\overset{o}{A}$ in (9,0) CNT with radius of 3.523 A. This fluctuation creates instability at the defect

similar to a notch and contributes to the strain concentration and lowering of stiffness.

Stiffness reduction at the defect not only affects the elastic behavior but, is also expected to alter the inelastic behavior. The elastic behavior (for example, Young's modulus) of a long nanotube with a few defects is marginally lowered because of relatively low area fraction of the defects. However, plasticity, fracture and failure are localized phenomena wherein the defects play a major role. It is now understood that the limiting behavior of nanotube either for onset of plasticity or for fracture is the generation of topological defects. Once the defects are nucleated they tend to serve as sites for further propagation of defects[36], or result in a crack propagation and brittle fracture[18] depending on various factors such as chirality and temperature[38]. Belytchko and coworkers[18] report that there is a reduction in fracture stress in presence of 5-7-7-5 defect, in addition defect serves as nucleation site for fracture. Defected regions of CNT experience higher strains for similar values of stress compared to defect free tubes. Lower stiffness of defect region studied here is a clear indication of reduced load carrying capacity. This causes higher localized strain concentrations responsible for failure at lower applied strains.

Local stiffness values of various CNTs with varying diameter are shown in Table II. It can be observed that there is very marginal difference in stiffness values for different (n,0) type of nanotubes (0.621 to 0.639 TPa). However, the stiffness of defect region in (5,5) nanotube (comparable in diameter to (9,0) CNT) is much lower (0.524 TPa). This indicates that curvature of nanotube plays a minimal role in determining the mechanical behavior of defected region. Lack of radial symmetry at the defect suggests anisotropic behavior of defect region. As a result stiffness of defect in (5,5) tube is lower than stiffness of other (n,0) type of tubes. It is interesting to note that formation energy[40] of defect is much higher for (5,5) nanotube (3.34 eV) than (n,0) type of nanotubes (2.12 - 2.75 eV).

V. CONCLUSION

This paper demonstrates that atomic level stress and strain measures can be used to determine the Young's modulus of carbon nanotubes. Further, these measures can be used effectively to evaluate the changes in mechanical behavior due to defects. Stiffness of defects reduces by about 30 to 50% and is dependent on a number of factors such as chirality, diameter and the loading conditions.

Acknowledgments

The authors wish to acknowledge the research collaborations with Professors Leon van Dommelen and Ashok Srinivasan during various phases of this work as a part of the Computational nanotechnology group at Florida State University. The funding provided by FSU Foundation is also gratefully acknowledged.

REFERENCES

[1]S. Iijima, Nature **354,** 56 (1991).

[2]T.W. Ebbesen and T. Takada, Carbon **33**, 973 (1995).

[3]B.I. Yakobson, C.J. Brabec and J. Bernholc, Phys. Rev. Lett. **76**, 2511 (1996)

[4]V.H. Crespi, M.L.Cohen and A.Rubio, Phys. Rev. Lett. **79**, 2093 (1997).

[5]T. Kostyrko, M. Bartkowaik and G.D. Mahan, Phys. Rev. B **59**, 3241 (1999).

[6]J.C. Charlier, T.W. Ebbesen and P. Lambin, Phys. Rev. B **53,** 11108 (1996).

[7]Z. Yao, H.W.C. Postma, L. Balents, C. Dekker, Nature **402,** 6759 (1999)

[8]M.P. Allen andW.J.Tildesley, Computer simulation of liquids, Oxford university press, Oxford, 1989.

[9]Z.S. Basinski, M.S. Duesberry and R. Taylor ,Canadian J.of Phys. **49,** 2160 (1971).

[10]J.F. Lutsko, J of Appl. Phys. **64,** 1152 (1988).

[11]J. Cormier, J.M. Rickman and T.J. Delph, J of Appl. Phys. **89**,99 (2001).

[12]K.S. Cheung and S. Yip, J of Appl. Phys. **70**, 5688 (1996).

[13]D. Brenner, Phys. Rev. B 42 (1990).

[14]W. Yu and A. Madhukar, Phys. Rev. Lett.79, 905 (1997)

[15]X.Y. Liu and J.B. Adams, Acta Mater. 46 (1998).

[16]S. Namilae,N. Chandra and T.G. Nieh, Scr. Mater. 46, 49 (2001).

[17]T. Halicioglu, Thin solid films 312, 11 (1998).

[18]T. Belytschko, S.P. Xiao, G.C. Schatz and R.S. Ruoff, Phys. Rev. B 65, 235430 (2002).

[19]Y. Xia, M. Zhao, Y. Ma, M Ying, X. Liu, P. Liu and L. Mei, Phys. Rev. B 65, 155415, (2002)

[20]B.A. Galanov, S.B. Galanov and Y. Gogotsi,, J of nanoparticle Res. 4, 207 (2002).

[21]O.C. Zienkiewicz, The finite element method, TMH publishing company limited, New Delhi, 1979.

[22]E. Hernandez,C. Goze, P. Bernier, and A. Rubio, Appl. Phys. A 68, 287 (1999).

[23]D. Qian,W.K. Liu, R.S. Ruoff, J of Phys. Chem. B 105, 10753 (2001).

[24]G. Zhou, W. Duan and B. Gu, Chem. Phys. Lett. 333, 344 (2001).

[25]A. Krishnan, E. Dujardin, T.W. Ebbesen, P.N. Yianilos and M.M.J. Treacy, Phys. Rev. B 58. 14013 (2001).

[26]J.P. Lu, Phys. Rev. Lett. 79, 1297 (1997)

[27]B.G. Demczyk,Y.M. Wang, J. Cumings, M. Hetman, W. Han, A. Zettl and R.O. Ritchie, Mater. Sci. and Eng. A 334, 173 (2002).

[28]G.V. Lier, C.V. Alsenoy,V.V. Doren and P. Gerrrlings, Chem. Phys. Lett. 326, 181 (2000).

[29]Z.C. Tu and Z.C.O. Yang, Phys. Rev. B 65, 233407 (2002).

[30]M.M.J. Treacy, T.W. Ebbesen, J.M. Gibbson, Nature 381, 678 (1996)

[31]J.P. Salveta, G.A.D. Briggs, J.M. Bonard, R. R. Bacsa, A.J. Kulik, T Stockli, Nancy A Burnham, and L Forro, Phys. Rev. Lett., 82 (1999)

[32]N. Yao, V. Lordi. Journal of Applied Physics, 84 (1998)

[33]C.F. Cornwell, and L.T. Wille , Solid State Communications, 101 555 (1997).

[34]D.H.Robertson, D.W.Brenner and J.W.Mintmire, Phys. Rev. B 45, 12592 (1992).

[35]B.I. Yakobson, C.J. Brabec and J.Bernholc, Phys. Rev. B 76, 2511 (1996).

[36]M.B. Nardelli, B.I. Yakobson and J.Bernholc, Phys. Rev. B 57, R4277 (1998).

[36]C. Wei, K.Cho and D. Srivastava, Phys. Rev. B 67, 115407 (2003).

[37]M.B. Nardelli, B.I. Yakobson and J.Bernholc, Phys. Rev. Lett., 81 4656 (1998)

[39]P. Zhang, P.E. Lammert and V.H. Crespi, Phys. Rev. Lett., 81 5346 (1998)

[40]B.C. Pan, W.S. Yang and J. Yang, Phys. Rev. B 62, 12652 (2000)

TABLE I. Values of Young's Modulus computed for CNT by different methods in the literature.

Author & Year	Method	Young's Modulus (TPa)	Other Material Parameters	Comments
Hernandez, Goze Bernier, Rubio (1998)	Total-energy, non-orthogonal tight binding, Axial tension	1.22 -1.26	Poisson's ratio: 0.18	wall thickness=0.34 nm $Y = V_o^{-1}(\partial^2 E/\partial \varepsilon^2)$
Timur Halicioglu (1998)	Molecular dynamics (Brenner's Pot) Axial tension	0.50	Poisson's ratio: 0.18	wall thickness=0.34 nm $Y = (\partial\sigma/\partial\varepsilon)_{\varepsilon=0}$
Dong Qian, Wing kam Liu and Rodney S Ruoff (2001)	Analytical method on graphene sheet	0.989	Poisson's ratio: 0.367	wall thickness=0.34 nm $C_{ijkl} = (\partial^2 W/\partial F_{ji}\partial F_{lk})$
Y Xia, M Zhao, Y Ma, M Ying, X Liu, P Liu and L Mei (2002)	Molecular dynamics and ab initio Internal pressure	C(5,5) 2.55(ε_{zz}<0.003) 0.85(ε_{zz}<0.04) 1.14(ε_{rr}<0.003) 0..52-0.26-(0.003<ε_{rr}<0.04)	Poisson's ratio used in calculation 0.17	Independent of wall thicknesss. Y increases with 5-7-7-5 defect
G Zhou, W Duan B GU (2000)	First principles cluster method (LDA) Axial tension	0.764	Poisson's ratio: 0.32	Tensile strength =6.249 GPa,
J P Lu (1997)	Emperical force constant model	0.971-0.975	Poisson's ratio: 0.277-0.280	wall thickness=0.34 nm
J M Molina, S S savinsky and N.V. Khokhriakov (1995)	Tight binding	1.4	----	wall thickness=0.34 nm
A. Krishnan, E. Dujardin T W Ebbesen, P N Yianilos and M M J Treacy (1998)	Experimental: free standing room temperature vibrations	1.25	-----	Weighted average value
B I Yakobson C J Brabec and J Bernholc, (2001)	Many body potential and continuum shell model	5.5	Poisson's ratio: 0.19	wall thickness=0.066 nm
B G Demczyk, YM Wang, J Cumings, M Hetman, W Han, A Zettl, RO Ritchie (2002)	:Experimental pull and bend test	0.91	Tensile strength =0.15 TPa	wall thickness=0.334 nm with continuum correction Young's modulus = 0.8TPA
Yu MF, Files BS, Arepalli S, Ruoff RS (2002)_	Experimental Tension test	0.32-1.47	Failure strength: 13-52 GPa	wall thickness=0.34 nm
Tu ZC abd Yang ZCO (2002)	LDA	4.7	Poisson's ratio: 0.34	wall thickness=0.075 nm
Lier GV, Alsenoy CV, Doren, VV, Geerlings P (2000)	Ab initio	0.72-1.120	Poisson's ratio: 0.026-0.125	wall thickness=0.34 nm
Treacy MMJ, Ebbesen TW, Gibbson JM (1996)	Experimental (TEM)	1.81	-----	First measurement of Y
Salveta JP, Briggs GAD, Bonard JM, Bacsa RR, Kulik AJ, Stockli T, Burnham NA, and Forro L (1999)	Experimental (Atomic Force Microscope)	1.0	Shear modulus = 1GPa,	wall thickness=0.34 nm
Yao N, Lordi V (1998)	Molecular Dynamics (Thermal vibrational frequencies)	1.0	----	wall thickness=0.34 nm
Cornwell CF, and Wille LT	Molecular Dynamics (axial Compression)	0.2 - 2.0	-----	Y varies with radius

TABLE II Stiffness of defected region of different nanotubes.

Nanotube	Radius(nm)	Chiral angle	Stiffness (TPa)
(9,0) (Defect Type I)	0.352	0^0	0.621
(9,0) (Defect Type II)	0.352	0^0	0.627
(10,0)	0.391	0^0	0.639
(11,0)	0.431	0^0	0.639
(13,0)	0.509	0^0	0.638
(15,0)	0.587	0^0	0.629
(5,5)	0.339	30^0	0.524

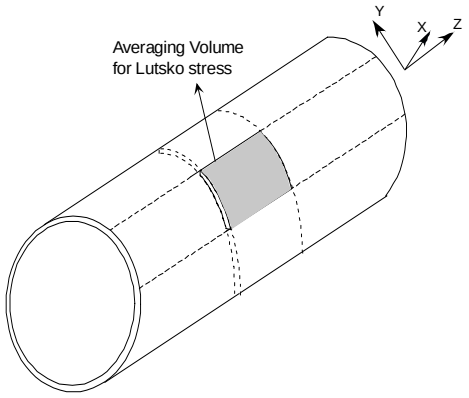

Figure 1: Averaging volume used for Lutsko stress in the simulations.

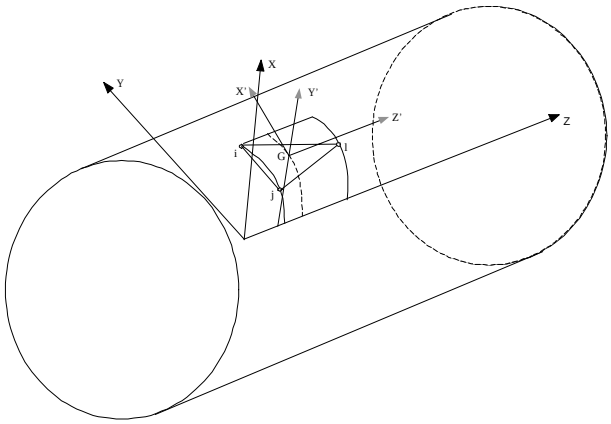

Figure 2: A typical triangular facet, with the local coordinates (x^0, y^0, z^0) coinciding with centroid of triangular element.

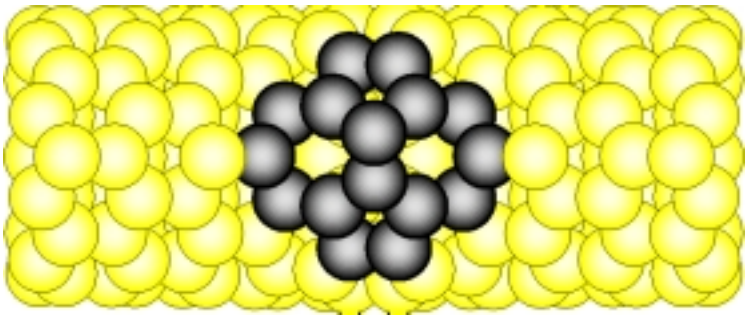

Figure 3: (9,0) tube containing 5-7-7-5 defect of type I.

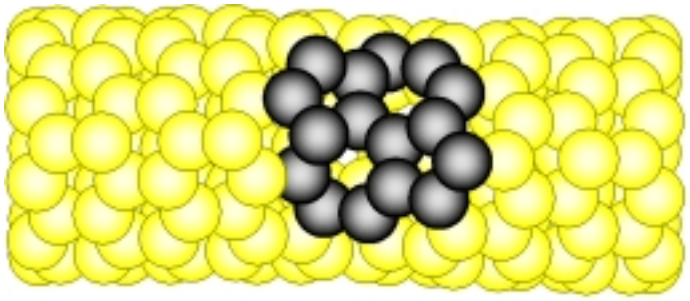

Figure 4: (9,0) tube containing 5-7-7-5 defect of type II.

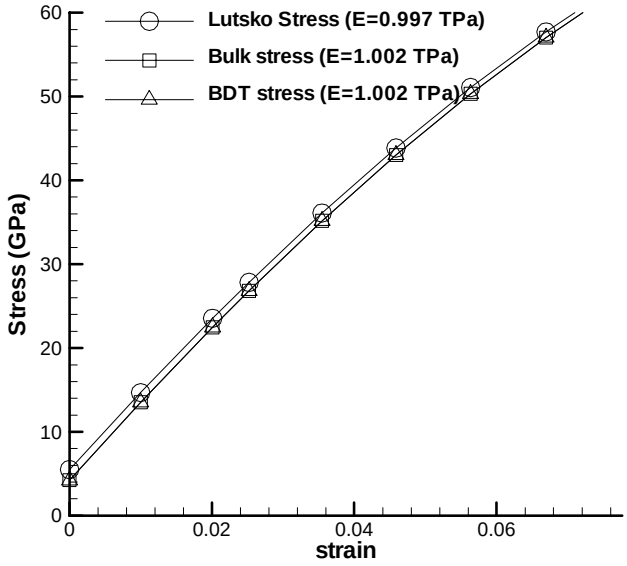

Figure 5: Stress-strain curve for (9,0) perfect tube subject to uniaxial tension based on three stress measures.

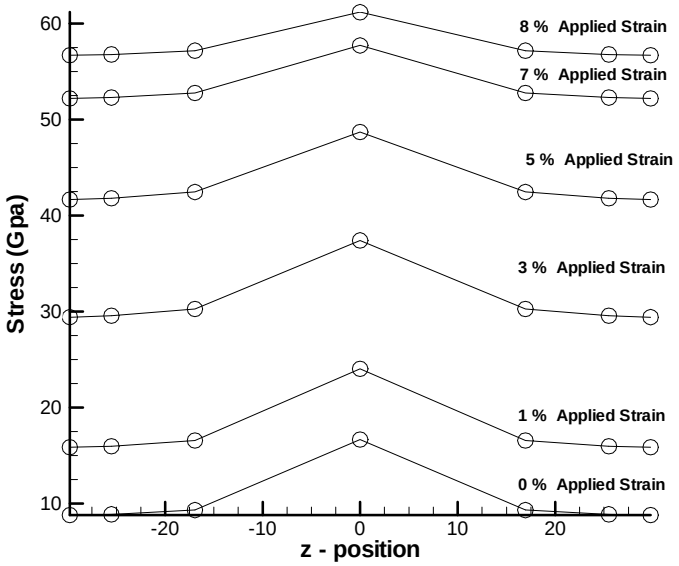

Figure 6: Variation of Lutsko's stress along the length of (9,0) SWCNT containing a 5-7-7-5 defect of type I near the center of tube.

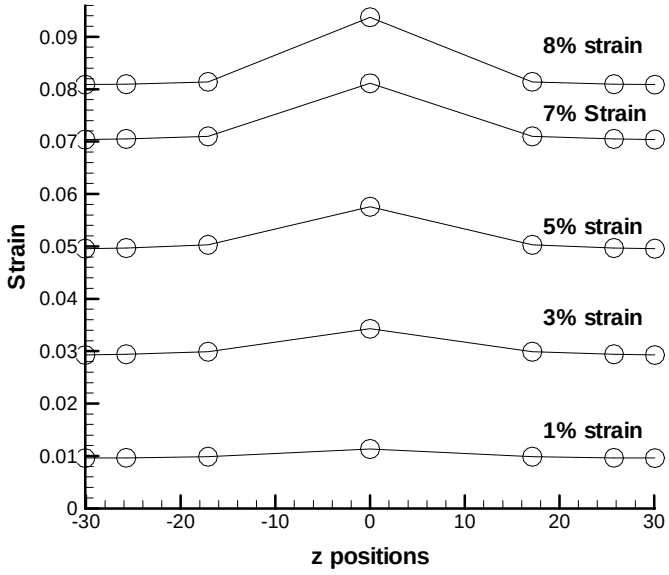

Figure 7: Variation of strain ε_{33} along the length of (9,0) SWCNT containing a 5-7-7-5 defect of type I near the center of tube.

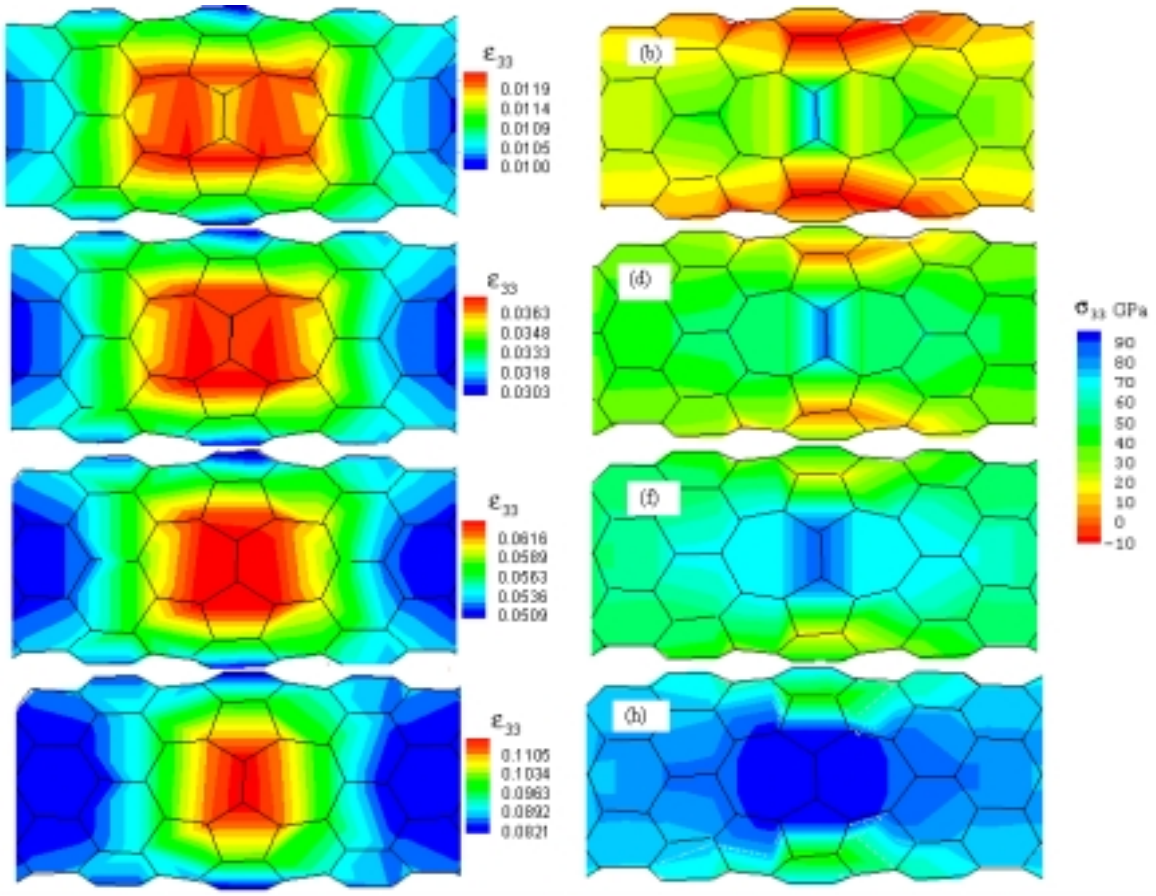

Figure 8: Contour plots of longitudinal strain ε_{33} strain and stress σ_{33} near the defected region drawn at different applied strain levels. (a) Strain contours at applied strain of 1%, (b) stress contours at applied strain of 1%, (c) strain contours at applied strain of 3%, (d) stress contours at applied strain of 3%, (e) strain contours at applied strain of 5%, (f) stress contours at applied strain of 5%, (g) strain contours at applied strain of 8%, (h) stress contours at applied strain of 8%.

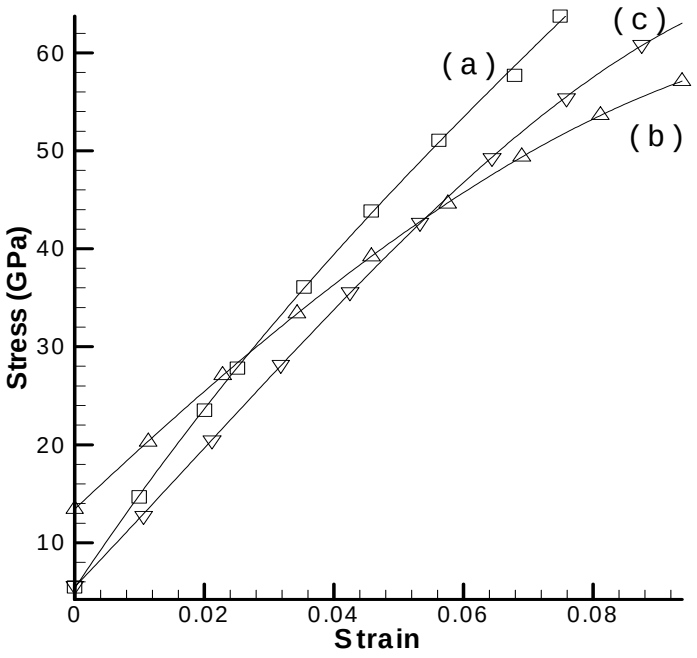

Figure 9: Stress-strain curves for (9,0) carbon tube with and without defect. (a) Stress-strain curve for tube without defect, (b) Stress-strain curve for type I defect and (c) Stress-strain curve for type II defect.

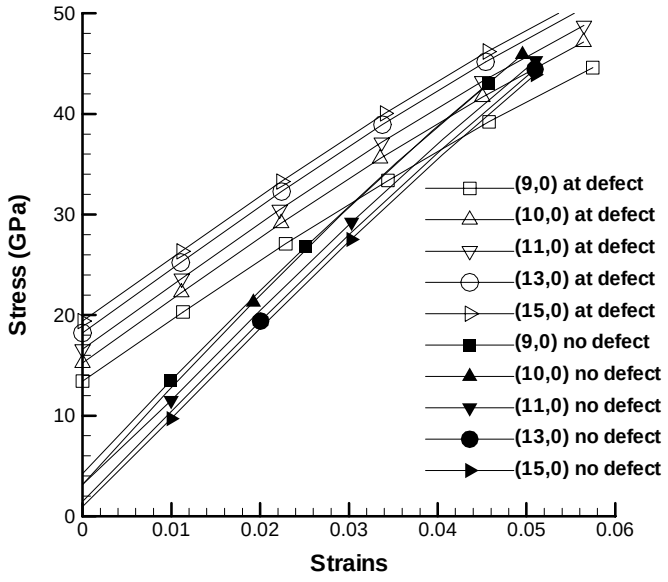

Figure 10: Stress-strain curves for tubes of different diameters with defect and without defect. Stress-strain curves with filled symbols are for tubes without defect and stress-strain curves with open symbols are for tubes with defect.

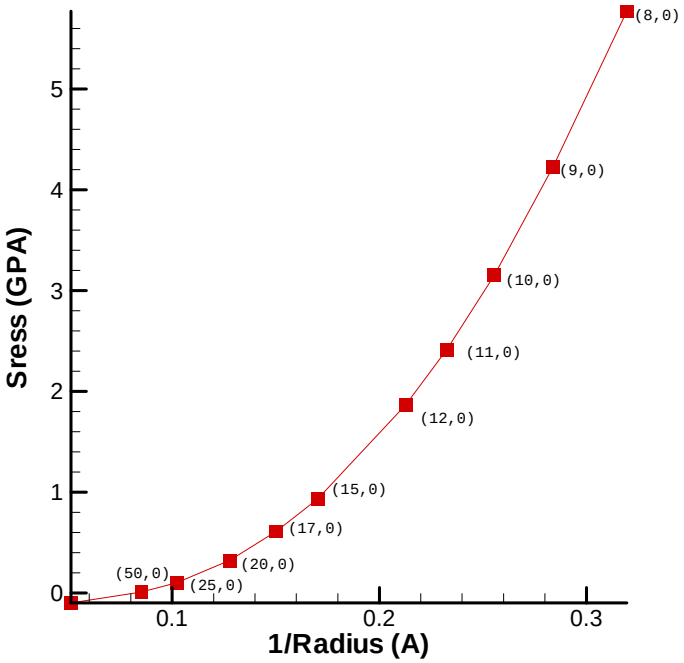

Figure 11: Residual stress variation with radius

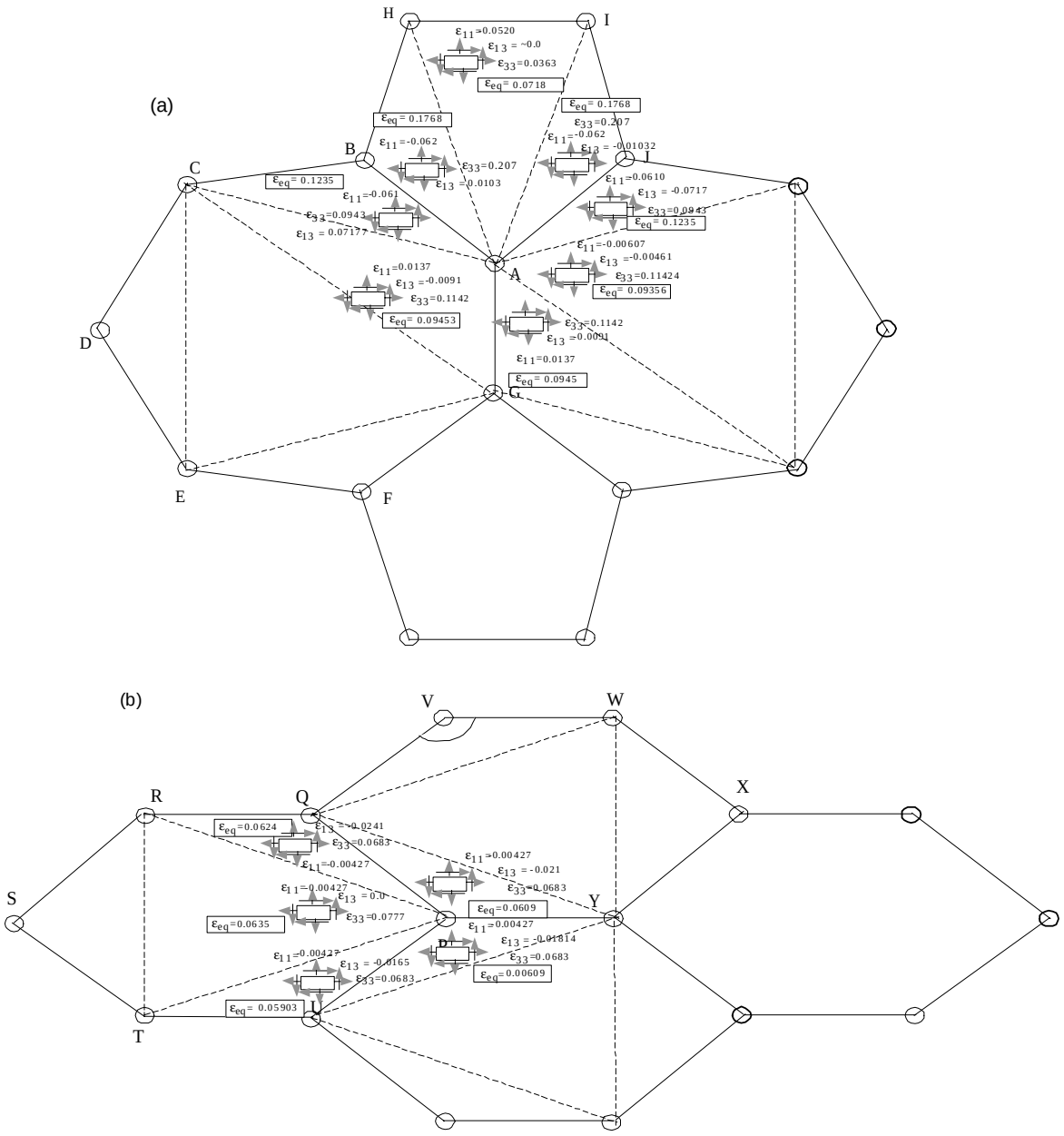

Figure 12: (a) Atomic configuration of 5-7-7-5 defect in (9,0) carbon nanotube with local variation of strains around one of the critical atom (b). Atomic configuration of perfect region far away from 5-7-7-5 defect in (9,0) carbon nanotube with local variation of strains around a typical atom. Dashed lines indicate subelement divisions.

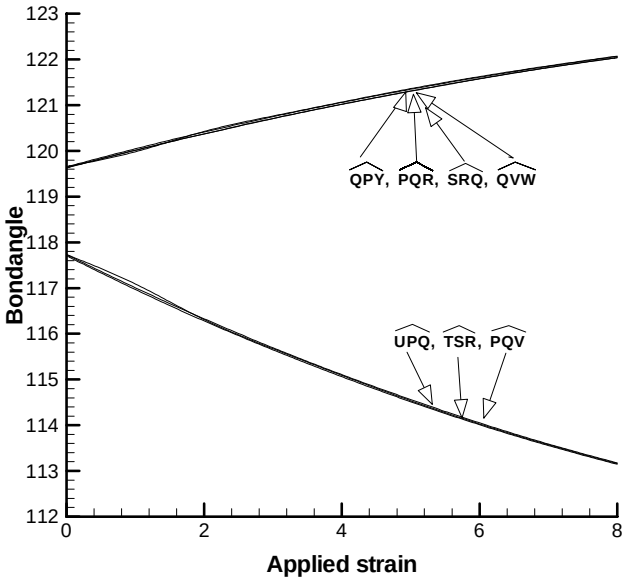

Figure 13: Bond angle variation with applied strain for few bond angles at perfect region away from the defect.

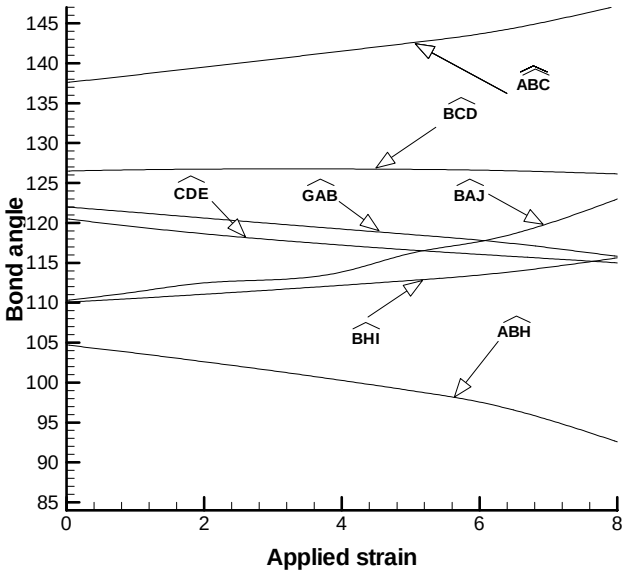

Figure 14: Bond angle variation with applied strain for few bond angles near defected region.